Nanoscale Path Planning and Motion Control with Maglev Positioners

Huzefa Shakir, *Student Member, IEEE*, and Won-Jong Kim, *Senior Member, IEEE*

***Abstract*—This paper addresses nanoscale path planning and motion control, which is essential in nanomanufacturing applications such as microstereolithography (μSTL), dip-pen-nanolithography (DPN), and scanning applications for imaging and manipulation of nanoscale surface phenomena, with the magnetic levitation (maglev) technology. We identified the motion trajectories commonly used in industrial applications along with the challenges in optimal path planning to meet the nanoscale motion-control objectives and achieve precise positioning and maximum throughput simultaneously. The key control parameters in path planning are determined, and control design methodologies, including a well-damped lead-lag controller and an optimal linear quadratic regulator are proposed to satisfy the positioning requirements. The proposed methodologies were implemented individually and collectively. The experimental results are presented in this paper to illustrate their effectiveness in planning optimal trajectories. The damped lead-lag controller exhibited the command overshoot values of as small as 0.37%, and the multivariable LQ controller reduced the dynamic coupling among the axes by 97.1% as compared with the decoupled single-input–single-output (SISO) lead-lag controllers. The position resolution of 5 nm was achieved in x and y with the errors in command tracking as small as 4.5 nm. The maglev stage demonstrated excellent performances for the chosen nanomanufacturing applications in terms of position resolution and accuracy, and speed.**

***Index Terms*—Maglev system, multivariable optimal control, nanomanipulation, nanomanufacturing, nanoscale path planning, precision positioning.**

I. Introduction

MANUFACTURING at nanoscale is one of the major research and development focus areas in the application of nanotechnology and has significant economic and societal impacts [1]. The development of the scanning tunneling microscope (STM) and the atomic force microscope (AFM) initiated a variety of atomic-level profiling and characterizing instruments [2]–[4]. These scanning probe microscopes (SPMs) were originally intended for molecular and atomic-level topographic imaging. In the last decade, however, the STM/AFM became one of the key instruments in nanoscale manipulation [5]. The fundamental limitation of the manipulation methodology with an STM/AFM is that these manipulators have only a limited two-dimensional (2-D) motion capability with small (several micrometers) vertical motion without rotational motion capabilities. Moreover, lead zirconate titanate (PZT) ceramics frequently used in the piezoelectric actuators of an STM/AFM has several major downsides, including thermal drift, hysteresis, limited linear range, and high operation voltage. Because of these drawbacks, these SPM-based manipulators alone cannot be used as nanomanufacturing tools. Thus, novel actuation and sensing mechanisms are needed to meet the demanding specifications in nanoscale manufacturing.

The magnetic levitation technology has been demonstrated successfully for nanopositioning applications. Several research groups developed precision positioning devices using this technology. Kim, Shan *et al.*, Holmes *et al.*, and Hajjaji *et al.* have done pioneering work in high-precision magnetic levitation [6]–[9]. Verma *et al.* describes in detail the maglev stage we use as a test bed in this paper [10]. The main benefit of magnetic levitation over other prevailing technologies is its noncontact nature while in operation, i.e., the forces are applied to the moving part without any mechanical contact. Thus, there is no friction, hysteresis, or backlash. This maglev technology is suitable for clean-room or vacuum environments, since it does not generate wear particles or requires no lubricants. Furthermore, without using complicated mechanical elements, the fabrication cost can be substantially reduced.

Despite the above discussed advantages of the magnetic levitation, it has several inherent technical challenges.

1) The maglev systems are open-loop unstable.
2) Since only a single moving part generates all the motions, its dynamics is coupled in six degrees of freedom (DoFs).
3) Owing to the absence of any damping or restricting force on the moving part, the overshoots to the commanded steps are large.
4) The nonlinear relationship between the current and displacement may not allow large travel ranges.

The working of maglev stages has largely been demonstrated in literature with basic closed-loop control. When put in conjunction with a practical application, the control requirement may be more stringent.

Various potential applications of the maglev nanopositioning device include microstereolithography (μSTL), dip-pen-lithography (DPN), scanning/imaging, atomic level manipulation, and nanoscale vibration isolation for delicate instruments. One of the most important tasks in these applications is nanomanipulation, which essentially requires positioning, orienting, and manipulating at nanoscale precision. Consequently, the maglev stage needs to be tested rigorously for set-point changes, and application-specific control strategies and motion planning need

Manuscript received September 4, 2005; revised April 12, 2006. Recommended by Technical Editor K. Ohnishi. This work was supported by the National Science Foundation under Grant CMS-0116642.

The authors are with the Department of Mechanical Engineering, Texas A&M University, College Station, TX 77 843-3123 USA (e-mail: huzefa@tamu.edu; wjkim@tamu.edu).

Digital Object Identifier 10.1109/TMECH.2006.882995

[1]National Nanotechnology Initiative. [Online]. Available: http://www.nano.gov/html/research/nnigc.html

to be devised to demonstrate its use as a precision positioning device in any of its applications. In such applications, this maglev stage will be used as a cluster tool for precision manufacturing, and all the processes can be completed with a fixed tool set.

In this paper, we develop several path planning techniques to reduce the large-overshoot problem. There are many research results on the macroscopic time-optimal control especially in path planning in robotics [11]–[13]. However, no significant literature is available for manufacturing the applications at nanoscale. We designed and implemented a multivariable linear quadratic regulator (LQR) for the lateral modes (x, y, and the angle about the z-axis) of the maglev stage to reduce the coupling among the axes [14]. Although we have used well-established classical and modern control techniques to design the controllers, our methodologies enable path-planning and motion-control at nanoscale.

This paper is organized as follows. Section II gives a brief description of the maglev stage. The concept of nanoscale path planning is introduced in Section III with basic trajectories to emulate real-life applications and to deal with the challenges in path planning and motion control at nanoscale. Section IV describes the design and implementation of a multivariable LQR motion controller for the lateral modes of the nanopositioning maglev stage to achieve a critically damped trajectory without compromising the rise and settling times. Experimental results for general trajectories relevant to nanomanufacturing using the proposed methodologies are presented and discussed in Section V.

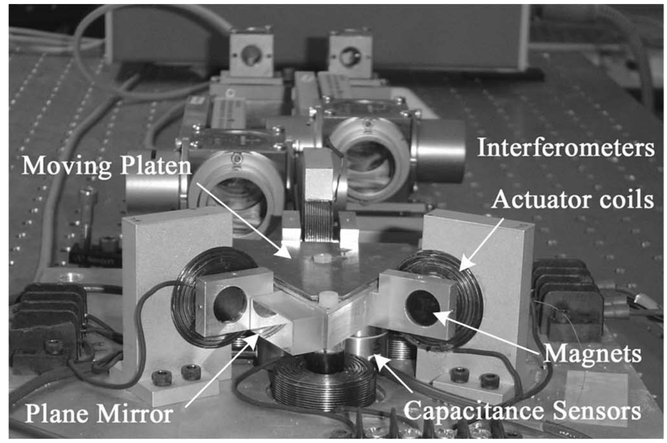

(a)

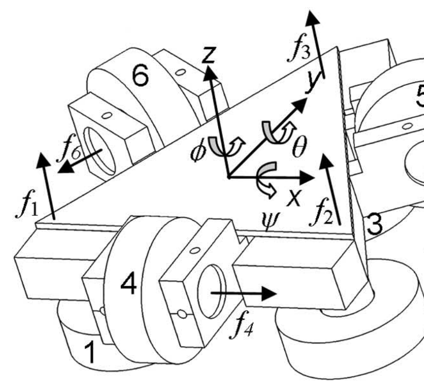

(b)

Fig. 1. (a) Photograph of the maglev stage. (b) Forces from each unit actuator and axes convention.

II. Maglev Stage Overview

A photograph of the mechanical assembly is shown in Fig. 1(a). A single moving part, namely the platen, consists of a triangular aluminum part pocket-milled to reduce the mass while maintaining the structural stiffness for high natural frequency. The total mass of the moving part is 0.212 kg, and the total power consumption by all the actuators is only about 1 W. There are six sets of magnets for six single-axis actuators. The coils for all six actuators are mounted on a stationary aluminum base plate via coil holders. The design of these single-axis actuators are described in Kim *et al.* [15]. There are three plane mirrors attached to the sides of the platen, and a horizontal motion sensing at subnanometer resolution is achieved with three laser interferometers. The sampling frequency of the laser interferometers is 250 kHz. For a vertical motion sensing, we have three capacitance gauges mounted on the base plate right below the platen. The six-axis motions are generated by the application of six independent force components. The positive directions of these forces are defined in Fig. 1(b). A combination of horizontal forces makes the platen move in x, y, and ϕ, and a combination of vertical forces makes it move in z, θ, and ψ. A detailed description of the mechanical and instrumentation structure can be found in [10].

III. Nanoscale Path Planning

Fig. 2(a) shows a motion trajectory (dashed line) followed by the platen that can be employed in a μSTL application with the controllers given in [10]. As shown in the figure, the actual path significantly overshot the commanded trajectory. This is because the controller was not optimized for speed, and the platen did not begin the corner turns until the actual path overshot the command. Furthermore, since the controllers were simple lead-lag compensators, there was no direct control over the velocity. Coupling between the x- and y-axes was also significant as seen in Fig. 2(a), since the controllers were SISO ones. In the following sections, several attempts are made to reduce these shortcomings for better trajectory tracking.

A. Overshoot Reduction

There are various ways through which the overshoot may be reduced.

1) *Using smaller yet uniform position-command steps:* Since the plant is assumed to be linear, the overshoot is proportional to the step size. Hence, the overall overshoot can be significantly reduced by using successive smaller position-command steps instead of a single large one. Fig. 2(a) shows the path (dash-dotted line) followed by the stage using smaller uniform steps of 5 μm against the larger 20 and 25 μm steps shown with the dashed line to cover the same distance. The errors in x are shown in Fig. 2(b) with large single steps (dashed line) and uniform smaller steps (dash-dotted line). The overall percentage overshoot was

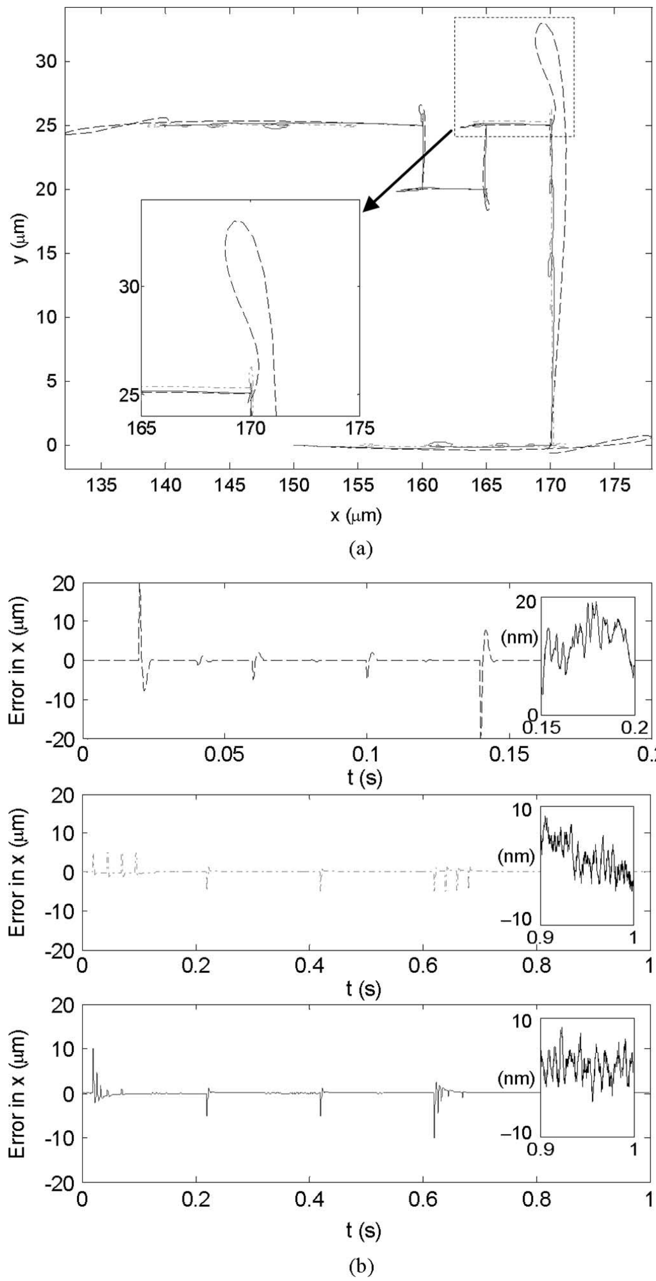

Fig. 2. (a) Path traversed by the platen without using path-planning methodologies (*dashed*), with smaller uniform steps of 5 μm (*dash-dotted*), and with decreasing step commands (*solid*). (b) Errors in the corresponding trajectories.

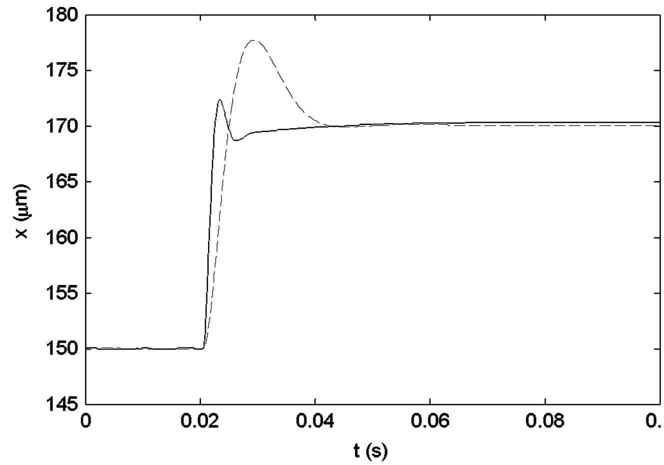

Fig. 3. Step responses in the x-axis with the 85.8-Hz (*solid*) and 47.5-Hz (*dashed*) controllers.

reduced from 39.35% to 6.58% in x, and from 31.99% to 5.05% in y. The percentage overshoot was calculated by dividing the maximum amount the platen overshoots its final value by its final value, expressed as a percentage.

2) *Using decreasing position-command steps:* An alternate method is to use decreasing step-command sizes. This, in effect, slows down the platen as it approaches the corners. Fig. 2(a) (solid line) shows the path followed by the stage using the step-sizes, which decrease in a geometric progression (12.5000, 6.2500, 3.1250, 1.5625, and 1.5625 μm). The error in x is shown in Fig. 2(b) with a solid line. The overall percentage overshoot was reduced prominently to 2.32% from 39.35% in x, and 2.12% from 31.99% in y.

The performance of the maglev positioner is almost identical in x and y and hence, the y-axis error results are omitted. Note that in all the three plots, the main source of error in the trajectory tracking is the sudden change in the commanded path around the corners, which is our main concern. In the steady state, the position resolution for the trajectories using the path planning methodologies remains better than 10 nm peak-to-peak. For the above two trajectory planning experiments, we used a controller with a 47.5-Hz crossover frequency and 51° phase margin (PM).

3) *Using a damped controller:* The above two methods, however, depend on the nature of the trajectory and provide little flexibility. Furthermore, applications like scanning demand a much better transient response and any overshoot is unacceptable. A better way to tackle the problem is to design a well-damped controller that gives a lesser overshoot. We designed another controller with a larger crossover frequency of 85.8 Hz and 73° PM to meet the conflicting requirements of lesser overshoot and faster dynamic responses simultaneously. The step responses in x with this controller and the one being used in the previous two methods (with a crossover frequency of 47.5 Hz and 51° PM) have been shown in Fig. 3. The percentage overshoot was reduced from 39.35% to 11.85%. Additionally, owing to the larger crossover frequency, the rise time decreased from 4.5 to 2.2 ms using a 10% criterion.

B. Velocity Control

Another parameter to be controlled in the trajectory tracking is the velocity. We need the platen to slow down as it approaches the corners [as shown in Fig. 2(a)] for sharper maneuver. Similarly, in the trajectories that require continuous directional changes, it is crucial to have precise control over the velocity in addition to the position. One way to control the velocity is, again, through controlling the command step size. The implementation of the controller in the form of difference

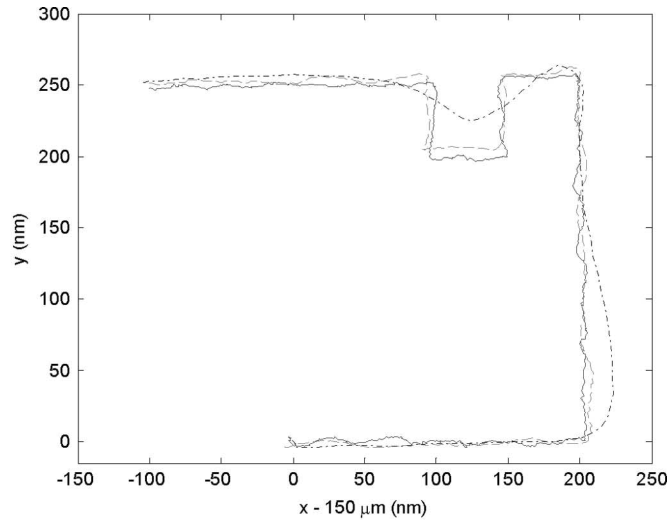

(a)

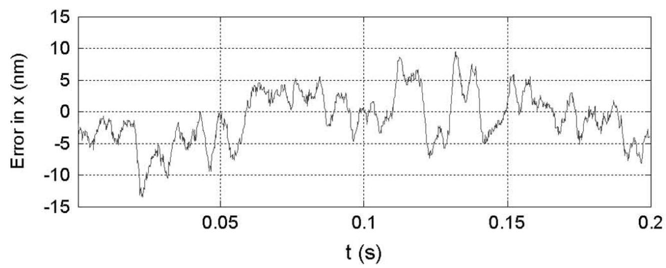

(b)

Fig. 4. (a) Paths traversed at various speeds by the platen at nanoscale–50 μm/s (*dash-dotted line*), 25 μm/s (*dashed line*), and 5 μm/s (*solid line*). (b) Error in x in the path traversed with 5 μm/s [*solid line* in part (a)].

equations requires steps at fixed-time intervals (0.2 ms in our case at the sampling rate of 5 kHz). Varying the step size for the fixed-time intervals is thus equivalent to varying the speed of the platen.

Fig. 4(a) shows the effect of varying the platen speed. It shows the same trajectory followed by the platen as shown in Fig. 2(a) but with the spatial scale reduction by a factor of 100. As the platen speed was reduced from 50 to 5 μm/s, the position accuracy of the platen was dramatically improved. Fig. 4(b) shows the error in x. The performance of the maglev positioner is almost identical in x and y and hence, the y-axis error results are omitted. The position-noise level varied from the best of 4.5 nm to the worst of 10.5 nm (peak-to-peak). The maximum deviation from the trajectory was 8.5 nm.

C. Nanoscale Trajectory Tracking

The above two methodologies combined together can drastically improve trajectory tracking. Fig. 5 shows the same trajectory followed using this combined path-planning methodology. The path was traversed at a constant velocity of 50 μm/s. A comparison between this trajectory and the one shown in Fig. 2(a) (dashed line) shows that the percentage overshoot was reduced from 39.35% to 0.45% in x, and 31.99% to 0.37% in y. The maximum steady-state error was reduced from 20.6 to 18.2 nm. However, the total time taken to trace

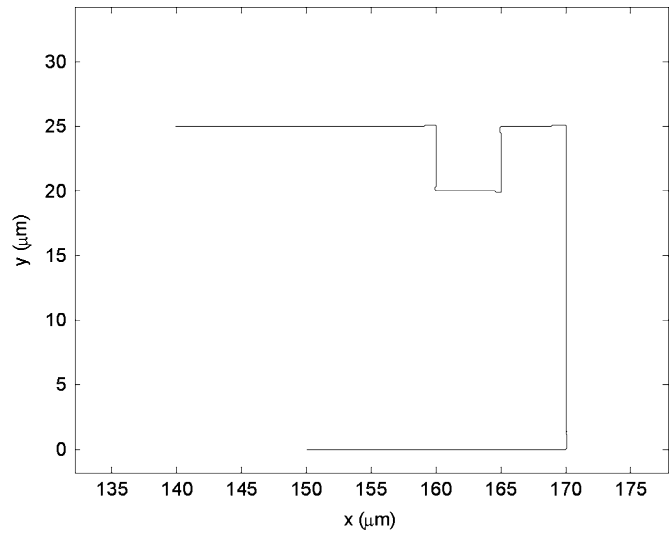

Fig. 5. Path traversed by the platen using the combined path-planning methodology.

the entire trajectory increased from 0.17 to 1.7 s. This time increase is, however, acceptable for an application like μSTL that works at a much slower rate [16].

IV. Multivariable LQ Control

Since there is only one moving part that generates all the six-DoF motions, its dynamics is coupled. The path-planning methodologies discussed above do not address this dynamic coupling, since the SISO controllers were designed assuming that the dynamics of the platen is decoupled in all six axes. Furthermore, direct velocity feedback was not used by the controllers. This gives rise to the need of designing an advanced controller, which has led to the development and implementation of a multivariable LQ control scheme for this purpose.

A. Plant Modeling and Linearization

In order to develop high-performance controllers, precise dynamic modeling is required. To start with, we decoupled the plant into two modes, vertical and lateral, against all the six decoupled axes used previously. We designed an LQR for the lateral modes (x, y, and angle about the z-axis, ϕ) and kept the decoupled SISO lead-lag controllers for the vertical modes (z, angle about the x-axis, ψ, and angle about the y-axis, θ). The reason for this choice is that we do not need to differentiate the position data or build a state estimator for velocity feedback for the lateral control, since full-state feedback is provided by the laser-interferometer electronics.

To apply the multivariable control, a state-space model of the platen dynamics was derived. The full equations of the motion are nonlinear because of the nonlinear current-force characteristics of the actuators as well as the dependence of the platen motion on the trigonometric functions of the angles of rotation with respect to the inertial frame. A detailed analysis and linearization was discussed in [14]. Here, we present the final state-space equations for the lateral mode.

$$\begin{bmatrix} \dot{\tilde{x}} \\ \dot{\tilde{y}} \\ \dot{\tilde{\phi}} \\ \dot{\tilde{u}} \\ \dot{\tilde{v}} \\ \dot{\tilde{r}} \end{bmatrix} = \begin{bmatrix} 0 & 0 & 0 & 1 & 0 & 0 \\ 0 & 0 & 0 & 0 & 1 & 0 \\ 0 & 0 & 0 & 0 & 0 & 1 \\ 0 & 0 & 0 & 0 & 0 & 0 \\ 0 & 0 & 0 & 0 & 0 & 0 \\ 0 & 0 & 0 & 0 & 0 & 0 \end{bmatrix} \begin{bmatrix} \tilde{x} \\ \tilde{y} \\ \tilde{\phi} \\ \tilde{u} \\ \tilde{v} \\ \tilde{r} \end{bmatrix} + \begin{bmatrix} 0 & 0 & 0 \\ 0 & 0 & 0 \\ 0 & 0 & 0 \\ 7.8921 & -3.9460 & -3.9460 \\ 0 & 6.8347 & -6.8347 \\ 287.2842 & 292.3645 & 297.4250 \end{bmatrix} \begin{bmatrix} \tilde{i}_4 \\ \tilde{i}_5 \\ \tilde{i}_6 \end{bmatrix}, \quad (1)$$

where i_4, i_5, and i_6 are the currents in coils 4, 5, and 6 as shown in Fig. 1(b). The tilde ($\sim$) above the state variables indicates that they are small-signal variables about an operating point.

B. Linear Quadratic Regulation for Lateral Control

With the pure-mass model without friction being used here, the plant-transfer function should have a double pole at the origin of the s-plane theoretically. However, in practice, the plant poles may not be located precisely at the origin, and consequently, there can be a nonzero steady-state error. To deal with this problem, the plant model was augmented with integrators to eliminate this steady-state error. In this case, since we are interested in the position command tracking, three integrators are used, each for x, y, and ϕ.

Consider the plant represented by the following differential equations in the state-space form

$$\dot{\boldsymbol{x}}_p = A_p \boldsymbol{x}_p + B_p \boldsymbol{u}_p, \qquad \boldsymbol{y}_p = C_p \boldsymbol{x}_p. \quad (2)$$

Defining the new state vector $\boldsymbol{\xi}_p$ as

$$\dot{\boldsymbol{\xi}}_p = \boldsymbol{y}_p = C_p \boldsymbol{x}_p, \quad (3)$$

we get the augmented system dynamics as

$$\begin{bmatrix} \dot{\boldsymbol{x}}_p \\ \dot{\boldsymbol{\xi}}_p \end{bmatrix} = \begin{bmatrix} A_p & 0 \\ C_p & 0 \end{bmatrix} \begin{bmatrix} \boldsymbol{x}_p \\ \boldsymbol{\xi}_p \end{bmatrix} + \begin{bmatrix} B_p \\ 0 \end{bmatrix} \boldsymbol{u}_p$$
$$\boldsymbol{y}_p = [C_p \quad 0] \begin{bmatrix} \boldsymbol{x}_p \\ \boldsymbol{\xi}_p \end{bmatrix}. \quad (4)$$

Define the performance index as

$$\boldsymbol{J}(\boldsymbol{x}(\cdot), \boldsymbol{u}(\cdot), t_0) = \int_{t_0}^{\infty} \left(\boldsymbol{u}^T(t) R \boldsymbol{u}(t) + \boldsymbol{x}^T(t) Q \boldsymbol{x}(t) \right) dt. \quad (5)$$

This time-invariant infinite-time regulator problem is a minimization problem to find an optimal control $\boldsymbol{u}_p^*$ to minimize $\boldsymbol{J}$. The solution of this problem is well known and can be found in texts on optimal control as in [17].

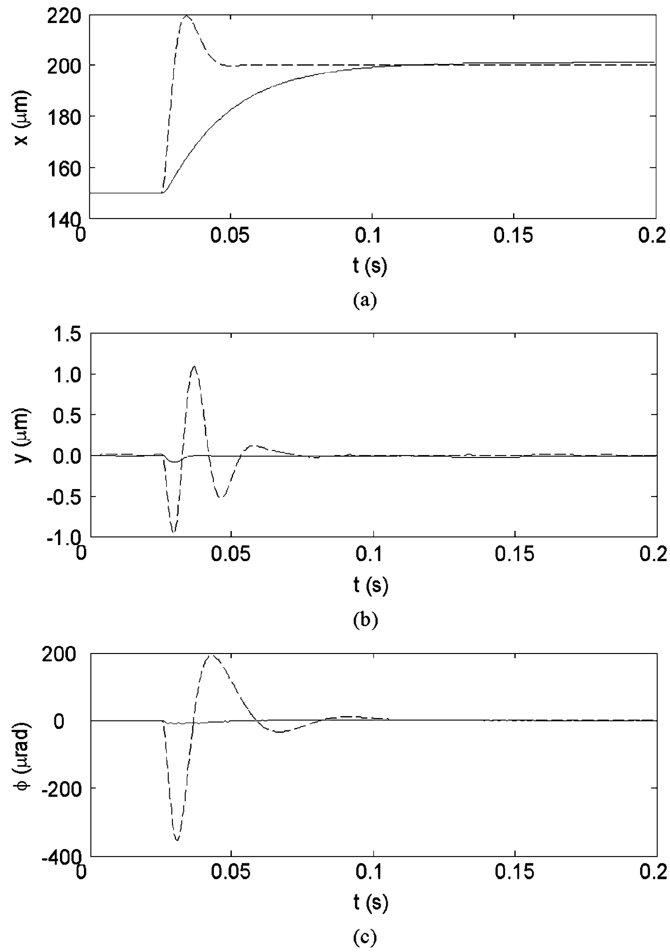

Fig. 6. (a) 50 μm step response in x. (b) Perturbation in y with the step in x. (c) Perturbation in rotation about z with the step in x. LQR (*solid line*), SISO lead-lag control (*dashed line*).

Fig. 6 compares the performances of the SISO lead-lag controller and the LQ controller for a 50 μm step response in x. The weight matrices for the LQ controller are given by

$$Q = \text{diag}\left([2\times 10^6 2 \times 10^6 2 \times 10^6 10^3 10^3 10^3 10^6 10^6 10^6] \right)$$
$$R = \text{diag}\left(0.1 \quad 0.1 \quad 10^3] \right) \quad (6)$$

Refer to [14] for the resultant LQ controller. The multivariable LQ control significantly reduced the dynamic coupling by 91.6% in y and 97.1% in ϕ as shown in Fig. 6(b) and (c). This reduction in the dynamic coupling was calculated by the percentage change in the maximum perturbation from the commanded position in y and ϕ, when a step-command is given in x. The developed multivariable optimal control requires greater rise and settling times as compared to the lead-lag control. However, the main objective was to reduce coupling among the axes, which was satisfactorily achieved as shown above. In practical applications, like μSTL, microscale assembly, scanning, indentation, etc., the processes themselves are much slower than the maglev positioner's dynamics. Thus, from a practical viewpoint, in spite of greater rise and settling times, the multivariable controller will still work well.

V. Test Results for Key Nanomanufacturing Applications

In this section, the proposed methodologies are applied to generate motion trajectories relevant to key nanomanufacturing applications such as DPN, μSTL, and scanning, and the effectiveness of the path-planning techniques is demonstrated. The physical properties and behavior of the material under manufacturing change at nanoscale. This scale-effect exists in a device, which is actually scaled down to a micro/nano-level size, for instance, an electrostatic microelectromechanical system (MEMS) motor. In our maglev system, however, there was no such physical scaling of the actual positioning device. The size of the moving platen is 115mm $\times$ 127mm $\times$ 12.7 mm. Owing to the benefits of the magnetic-levitation technology, we are able to achieve nanoscale path planning and motion control. Thus, by considering the facts that: 1) the forces acting on the positioner are too small (to the order of a few millinewtons) to produce any significant distortion in the structure of the platen, and 2) the laser-interferometer sensor provides averaged measured data over the beam diameter and because of multiple passes on the reflecting surfaces, we may conclude that the platen structure is rigid for all practical purposes. Hence, each point on the entire platen actually moves by exactly the same amount when the sensor senses the movement of a point on the platen.

A. Dip-Pen-Nanolithography

One of the practical applications that require extensive nanoscale path planning is DPN. DPN has emerged as an ideal solution for the direct-write nanofabrication, which plays an important role in areas such as sensor patterning, miniaturization of biological assays, and creation of nanoelectronic components. Nanoink uses NSCRIPTOR, a dedicated scanning probe lithography system, for the DPN process. Its scanning stage is motor-driven, and hence, requires intensive maintenance and suffers losses because of the friction from its contact-type mechanisms [18]. Besides, this apparatus uses seven motors for translation and zoom against the single-moving-part approach of the maglev stage designed by us. Furthermore, their scanning is performed by three independent piezos, which have several disadvantages over the maglev positioners as discussed in Section I. For instance, the total travel range is limited by 90 μm in x and y, and 8 μm in z. The placement precision is around 10 nm compared to 5 nm demonstrated by the maglev nanopositioner. Thus, our maglev system is much simpler and provides competitive advantages in terms of travel range, precision, and repeatability in DPN and other similar applications. Additionally, the maglev positioner can be used as a cluster tool in such applications, thereby eliminating the need for separate actuators for the positioning stage and cantilever probes. Thus, the probes can remain fixed throughout the entire patterning operation, while all the motion generations, as described below, can be performed using the maglev positioner.

DPN process employs microfluidic ink delivery devices, called DPN inkwells, for coating. The use of these microwells allows dipping the probe in ink in a controlled fashion, preventing the ink from coating the top side of the probe cantilever. A number of different inks can be simultaneously introduced on adjacent cantilevers in a probe array. A typical nanopatterning process consists of the following steps.[2]

- Step 1) The cantilever probe needs to be aligned with the microwells. The probe may be a single one or a probe array.
- Step 2) The probe is dipped in a microwell for coating. When lowering the probes onto the microwells, the probes contact the ink and their cantilevers bend. Here again, the lowering must be precisely controlled in order to avoid damage to the cantilevers.
- Step 3) After a successful dipping step, inking is complete. The probes are now translated onto the DPN substrate, where ink deposition can commence. Feature size is a primary concern for any patterning technology and can be controlled by regulating the amount of ink and the environmental conditions for transferring the ink to the substrate. The amount of ink, in turn, can be controlled by regulating the probe speed. As small as 80-nm line-width may be achieved with a write speed of 20 μm/s [18]. Also, for high-volume work where re-inking is necessary during the patterning process, the probes need to be switched repeatedly between the microwells and the substrate with the same level of position accuracy.

Apparently, all these steps require extensive path planning and motion control strategies. Fig. 7(a) shows the plot of experimental data of a trajectory traversed by the maglev platen for nanoscale patterning. The entire trajectory was traversed at variable speeds—20 μm/s for the write-speed channels, 100 μm/s for probe insertion, and 500 μm/s for probe release. The total time taken to complete this trajectory was 0.8 s. The height variation of the maglev positioner for patterning and rapid motions is shown in Fig. 7(b). Thus, all the three axis motions can be achieved using the single-part platen while the cantilever probe remains fixed throughout the nanolithographic process. This eliminates the need for a separate bias control for cantilever probes.

B. Microstereolithography

With its inception in the early 1990s, remarkable research progress has been made in MEMS. Many MEMS device concepts were proposed, and their feasibilities were demonstrated for applications in various fields of microfluids, aerospace, biomedical, chemical analysis, wireless communications, data storage, display, optics, etc. [19]. Manufacturing processes such as μSTL, micromachining, micromolding, and soft-lithography played a crucial role in the miniaturization of MEMS devices. Classical stereolithography (STL) processes use a laser beam deflected by a pair of low-inertia-galvanometric mirrors and focused by a dynamic lens to solidify the photopolymer [16]. This methodology works well for objects on the order of a few hundred micrometers. However, beam defocusing becomes problematic for smaller objects. This limits the minimum achievable

[2] Nanoink Inc. [Online]. Available: http://www.nanoink.net

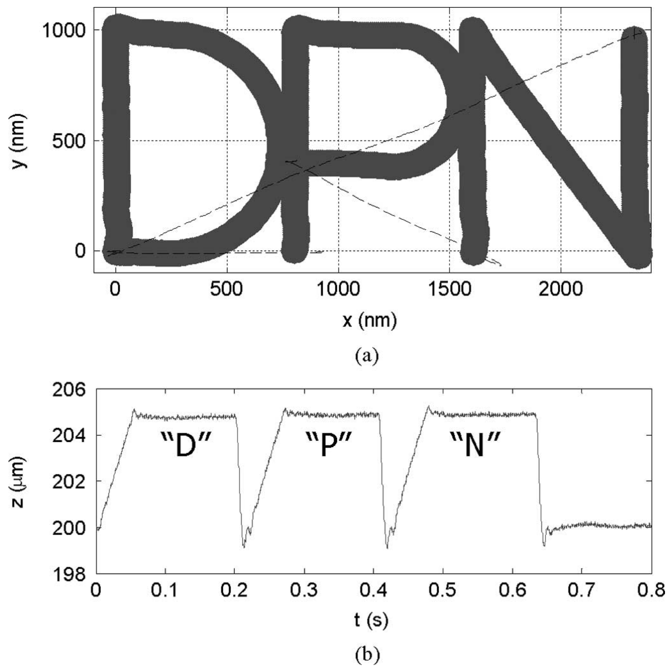

Fig. 7. (a) A DPN profile traced by the maglev nanopositioner at a write speed of 20 μm/s. The marker size is chosen so that the letters appear 80 nm wide in proportion to the size of the DPN pattern. Dashed lines represent the rapid motion of the stage while the probe is not in contact. (b) z-axis motion of the maglev platen with the nominal vertical position at 200 μm when the probe is not in contact with the substrate. The height of 205 μm corresponds to the platen's vertical position during the patterning processes of each letter, D, P, and N.

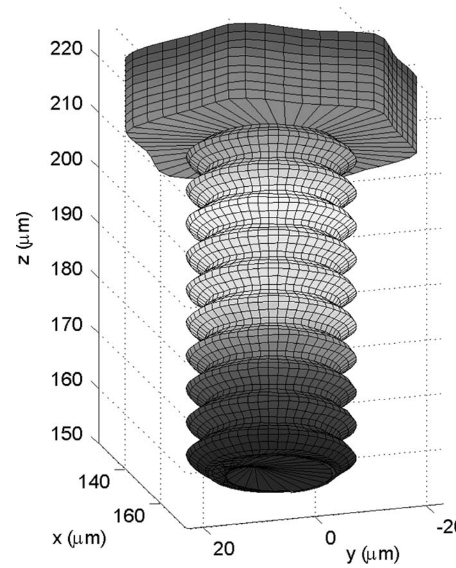

Fig. 8. A 3-D profile traced by the platen to manufacture a microscale screw for medical tissues with μSTL.

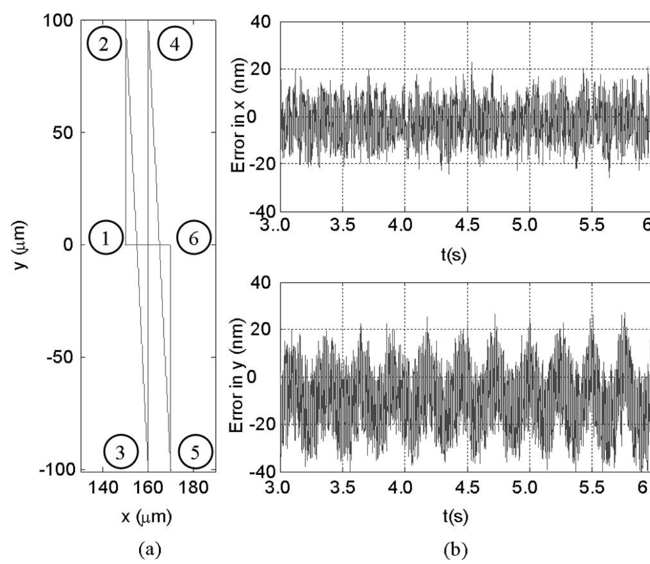

Fig. 9. (a) Active-scan and retrace sections scanned by the platen. (b) Errors in x and y.

component size. An alternate approach is to keep the laser beam fixed and use a high-precision positioning stage to generate x-y motions for scanning [19]. Magnetic levitation became an enabling technology for these applications with position resolution as good as 5 nm [10].

Fig. 8 shows a microscale screw for medical tissues traced by our maglev stage with the lateral resolution of 5 nm and vertical resolution of 100 nm. The inner radius, the outer radius, the pitch, and the length of the threads are 10.00, 13.75, 6.00, and 13.50 μm, respectively. The state of the art is the one fabricated by the Central Microstructure Facility with a lateral and vertical resolution of 10 μm, inner radius of 600 μm, thread length of 900 μm, and pitch of 150 μm, approximately [20]. Thus, our maglev positioner is capable of tracing the profile with a position resolution 2000 times better and the feature size 60 times smaller (comparing the inner diameters) as compared to the prevailing technology. Therefore, in such applications, the limitation on the minimum achievable size is posed by the manufacturing technology and not the positioning stage.

C. Scanning Applications

Among the commonly used scanning devices are: 1) piezo-based scanners to position a probe on a sample surface during the imaging of nanoscale surface phenomena with SPMs and 2) MEMS-based scanners to position the optical micromirrors in wearable computers [11]. An alternative is to keep the probe fixed and move the stage in the *xy*-plane to scan the surface.

A typical scanning operation consists of two sections: 1) the active-scan or output-tracking section where a desired output trajectory is prespecified and must be tracked precisely, and 2) the retrace or output-transition section where trajectory tracking is not critical. Instead, the output is to be returned to a predefined value so that the active scan can be repeated [11]. These active-scan and retrace sections are often repeated in a scanning operation. Fig. 9 shows a simple scanning trajectory traced by the maglev platen and the errors in x and y for the active-scan component to demonstrate its precision scanning capability in the active-scan section as well as the fast return motion in the retrace section. Paths 1-2, 3-4, and 5-6 are active-scan trajectories, and paths 2-3, 4-5, and 6-1 are fast retrace trajectories. The error in the active-scan section is well within 40 nm peak-to-peak in x and 60 nm peak-to-peak in y. The tracking speed and the return speed are 50 and 500 μm/s, respectively.

VI. Conclusion

With the recent development in nanomanipulation and nanomanufacturing, appropriate path-planning techniques are required as much as precision positioning itself. Although substantial research results are available on macroscopic trajectory planning and control, particularly in robotic applications, not much work has been reported yet in nanoscale path planning and motion control. In this paper, we investigated the key problems we may face while actually putting in use the nanomanipulation devices, more specifically, incorporating a maglev stage in manufacturing or scanning applications at nanoscale.

The parameters that influence the dynamic behavior of the positioning device were identified, and ways to control these parameters were proposed. The design and implementation of a well-damped SISO lead-lag controller and a multivariable LQ controller was described, and their influence on the performance of the maglev stage was discussed. Increasing the damping and reducing the velocity decreased the overall percentage overshoot from 39.35% to 0.45% in x and from 31.99% to 0.37% in y while cornering, thereby improving the dynamic performance significantly. The use of multivariable control ensured 91.6% lesser coupling in y and 97.1% in ϕ.

The test results for key nanomanufacturing applications such as μSTL, DPN, and scanning were presented. A position resolution of 5 nm in x and y was achieved, and the errors in command tracking were well within 40 nm peak-to-peak with the best performance of 4.5 nm. The minimum achievable feature size is thus limited only by manufacturing techniques and not by the positioning technology. The experimental results demonstrated that the maglev stage performed well for these nanomanufacturing applications in terms of position resolution, accuracy, speed, and versatility.

Acknowledgment

The authors thank J. Gu and S. Verma, former graduate students of W.-J. Kim, for their contributions in design, assembly, and software development for the maglev test bed.

References

[1] H. Doumanidis, "The nanomanufacturing programme at the National Science Foundation," *Nanotechnol.*, vol. 13, no. 3, pp. 248–252, Apr. 2002.

[2] G. Binning, H. Roher, C. H. Gerber, and E. Weibel, "Surface studies by scanning tunneling microscopy," *Phys. Rev. Lett.*, vol. 49, no. 1, pp. 57–61, Jul. 1982.

[3] G. Binning, C. F. Quate, and C. H. Gerber, "Atomic force microscope," *Phys. Rev. Lett.*, vol. 56, no. 9, pp. 930–933, Mar. 1986.

[4] R. M. Taylor, II, "The nanomanipulator: A virtual-reality interface to a scanning tunneling microscope," Ph.D. dissertation, Univ. North Carolina, Chapel Hill, NC, May 1994.

[5] L. T. Hansen, A. Kuhle, A. H. Sorensen, J. Bohr, and P. E. Lindelof, "A technique for positioning nanoparticles using an atomic force microscope," *Nanotechnol.*, vol. 9, no. 4, pp. 337–342, Dec. 1998.

[6] W.-J. Kim, "High-precision planar magnetic levitation," Ph.D. dissertation, Dept. Elect. Eng. Comput. Sci., Massachusetts Inst. Technol., Cambridge, MA, Jun. 1997.

[7] X. Shan, S.-K. Kuo, J. Zhang, and C.-H. Menq, "Ultra precision motion control of a multiple degrees of freedom magnetic suspension stage," *IEEE/ASME Trans. Mechatronics*, vol. 7, no. 1, pp. 67–78, Mar. 2002.

[8] M. Holmes, R. Hocken, and D. L. Trumper, "The long-range scanning stage: A novel platform for scanned-probe microscopy," *Precision Eng.*, vol. 24, no. 3, pp. 191–209, Jul. 2000.

[9] E. Hajjaji and M. Ouladsine, "Modeling and nonlinear control of magnetic levitation systems," *IEEE Trans. Ind. Electron.*, vol. 48, no. 4, pp. 831–838, Aug. 2001.

[10] S. Verma, W.-J. Kim, and J. Gu, "Six-axis nanopositioning device with precision magnetic levitation technology," *IEEE/ASME Trans. Mechatronics*, vol. 9, no. 2, pp. 384–391, Jun. 2004.

[11] H. Perez, Q. Zou, and S. Devasia, "Design and control of optimal scan trajectories: Scanning tunneling microscope example," *J. Dyn. Syst., Meas. Control*, vol. 126, no. 1, pp. 187–197, Mar. 2004.

[12] H. Chen, N. Xi, and Y. Chen, "Multiobjective optimal robot path planning in manufacturing," in *Proc. Intell. Robots Syst.*, 2003, vol. 2, pp. 1167–1172.

[13] K. Nakashima, T. Tsujino, and T. Fujii, "Multivariable control of a magnetic levitation system using closed-loop identification and H_∞ control theory," in *Proc. 35th Conf. Decision Control*, 1996, vol. 4, pp. 3668–3673.

[14] H. Shakir, W.-J. Kim, and S. Verma, "System identification and optimal control of a 6-DoF magnetic levitation stage with nanopositioning capabilities," in *ASME Int. Mech. Eng. Congr. Expo. 2004*, Anaheim, CA, Paper 60507, Nov. 2004.

[15] W.-J. Kim, H. Maheshwari, and J. Gu, "Maglev linear magnetic actuator for nanopositioning," in *ASME Int. Mech. Eng. Congr. Expo. 2002*, Orleans, LA, Paper 33395, Nov. 2002.

[16] P. F. Jacobs, *Stereolithography and Other RP&M Technologies*. New York: ASME, 1996.

[17] S. Stogestad and I. Postlewaite, *Multivariable Feedback Control*. New York: Wiley, 2003.

[18] D. Bullen, X. Wang, J. Zou, S. Hong, S-W. Chung, K. Ryu, Z. Fan, C. Mirkin, and C. Liu, "Micromachined arrayed dip pen nanolithography probes for sub-100 nm direct chemistry patterning," in *Proc. IEEE 16th Annu. Int. Conf. Micro Electro Mech. Syst.*, 2003, pp. 4–7.

[19] V. K. Vardan, X. Jiang, and V. V. Vardan, *Microstereolithography and Other Fabrication Techniques for 3D MEMS*. New York: Wiley, 2001, pp. 111–127.

[20] R. Lawes, (2002, Dec. 10). Microfabrication cost models for micromachining methods. Central Microstructure Facility, [Online]. Available: http://www.cmf.rl.ac.uk/latest/msl.html

Huzefa Shakir (S'02) received the B.Tech. (with honors) degree in mechanical engineering from the Indian Institute of Technology, Kharagpur, India, in 2000. He is currently working toward the Ph.D. degree at Texas A&M University, College Station.

In September 2002, he joined the Precision Mechatronics and Nanotechnology Laboratory, Department of Mechanical Engineering, Texas A&M University, where he is currently working as a Graduate Assistant. He has also worked as a Teaching Assistant for one year for the dynamic systems and controls related courses. He has worked as an Assistant Manager in Maruti Udyog Limited/Suzuki Motor Corporation, India, for two years after receiving the B.Tech. degree. His current research interests include analysis and design of control systems, nanoscale motion control, system identification, precision positioning systems, and bioinstrumentation.

Mr. Shakir is a student member of the American Society of Mechanical Engineers (ASME), and the Honor Society of Phi Kappa Phi and a Fellow of the Center for Teaching Excellence, Texas A&M University. He was a recipient of International Texas Public Education Grant 2006 and the Best Presentation Award in the American Control Conference 2005.

Won-Jong Kim (S'89–M'97–SM'03) received the B.S. (*summa cum laude*) and the M.S. degrees in control and instrumentation engineering from Seoul National University, Seoul, Korea, in 1989 and 1991, respectively. He received the Ph.D. degree in electrical engineering and computer science from the Massachusetts Institute of Technology (MIT), Cambridge, in 1997.

In September 2000, he joined the Department of Mechanical Engineering, Texas A&M University (TAMU), College Station, where he is currently Associate Professor. He was with the SatCon Technology Corporation, Cambridge, MA, for three years after receiving the Ph.D. degree. He holds three U.S. patents on precision positioning systems. His teaching and research interests include analysis, design, and real-time control of mechatronic systems, networked control systems, and nanoscale engineering and technology.

Dr. Kim received the Grand Prize from the Korean Institute of Electrical Engineers' Student Paper Contest in 1988. His 1997 MIT dissertation earned him the Gold Prize from Samsung Electronics' Humantech Thesis Prize. He was a semifinalist of the National Institute of Standards and Technology (NIST) Advanced Technology Program 2000 Competition. The National Aeronautics and Space Administration (NASA) granted him the Space Act Award in 2002. He was appointed a Select Young Faculty Fellow by TAMU College of Engineering and the Texas Engineering Experiment Station twice in 2003 and 2005. He received the Professional Engineering Publishing Award for the best paper published in the 2004 volume of the *Journal of Engineering Manufacture* in 2005. He is Chair of the American Society of Mechanical Engineers (ASME), ASME Nanoscale Control Technical Panel and Member of the IEEE Nanotechnology Council. He is a member of Pi Tau Sigma and ASME.